Magnetic reconnection during flux conversion in a driven spheromak

E. B. Hooper,[a] T. A. Kopriva,[b] B. I. Cohen, D. N. Hill, H. S. McLean, R. D. Wood, and S. Woodruff[c]
Lawrence Livermore National Laboratory, 7000 East Avenue, Livermore, California 94550

C. R. Sovinec
University of Wisconsin, 1500 Engineering Drive, Madison, Wisconsin 53706

(Received 9 June 2005; accepted 2 August 2005; published online 9 September 2005)

During buildup of a spheromak by helicity injection, magnetic reconnection converts toroidal flux into poloidal flux. This physics is explored in the resistive magnetohydrodynamic code, NIMROD [C. R. Sovinec, A. H. Glasser, T. A. Gianakon, D. C. Barnes, R. A. Nebel, S. E. Kruger, D. D. Schnack, S. J. Plimpton, A. Tarditi, and M. S. Chu, J. Comp. Phys. **195**, 355 (2004)], which reveals negative current sheets with $\lambda=\mu_0\mathbf{j}\cdot\mathbf{B}/B^2$ reversed relative to the applied current. The simulated event duration is consistent with magnetic diffusion on the sheet thickness and is accompanied by cathode voltage spikes and poloidal field increases similar to those seen in the Sustained Spheromak Physics Experiment, SSPX [E. B. Hooper, L. D. Pearlstein, and R. H. Bulmer, Nucl. Fusion **39**, 863 (1999)]. All magnetic field lines are open during reconnection and their trajectories are very sensitive to their starting points, resulting in chaos. The current sheets are most intense inside the separatrix near the *X* point of the mean-field spheromak, suggesting that the reconnection occurs near field lines which are closed in the azimuthal average. © *2005 American Institute of Physics*. [DOI: 10.1063/1.2040207]

I. INTRODUCTION

The reconnection of magnetic fields in space and astrophysical plasmas plays an essential role in their characteristics and evolution. Reconnection is also fundamental for the formation and evolution of laboratory plasmas such as the spheromak and reversed-field pinch, albeit at very different plasma parameters from those in the natural environment. Clearly, understanding the role and characteristics of the reconnection in these laboratory plasmas is important to their development and to elucidating the fundamental processes. Here we consider them in the context of a spheromak plasma.

A flux-core spheromak can be formed and sustained by a coaxial plasma gun, a process often called coaxial helicity injection.[1] The injection of magnetic energy and of helicity, a measure of linked magnetic fluxes, results when the voltage on the gun is applied across a bias poloidal magnetic flux between the gun and a "flux conserver."[1,2] The current from the gun generates a toroidal magnetic field and net toroidal flux. The resulting plasma configuration pinches and becomes unstable to nonaxisymmetric, magnetic modes with the $n=1$ toroidal mode usually dominant. In the low-amplitude, linear phase these modes generate poloidal magnetic field but the modes are nonsymmetric and no net, toroidally averaged poloidal flux is generated. However, when the mode amplitudes become large, nonlinear processes generate axisymmetric ($n=0$) poloidal field and flux, resulting in an amplification of the bias flux.[3,4] The generation of the axisymmetric flux requires a topological change in the field-lines via magnetic diffusion or reconnection.

The buildup of poloidal flux in the Sustained Spheromak Physics Experiment[5,6] (SSPX) is accompanied by voltage spikes on the gun cathode. Similar voltage spikes (or oscillations) were seen in the Compact Torus Experiment, CTX, when it was driven by a high impedance power source,[7] but their cause was not understood. The results presented in the present paper show that voltage spikes accompany magnetic reconnection in a resistive magnetohydrodynamic (MHD) simulation using the three-dimensional NIMROD code[8,9] which provides a description of the reconnection physics within the resistive MHD approximation.

Previous simulations show that the nonideal resistive MHD model with temperature-dependent resistivity, anisotropic temperature-dependent thermal conductivity, and Ohmic heating provides a good description of the macroscopic characteristics of the experiment.[10,11] For different SSPX shots and different NIMROD simulations, the following data are compared in Ref. 11: gun voltage and the flux-conserver edge poloidal magnetic field versus time; the peak electron temperature versus time; the relative fluctuation levels in the poloidal magnetic field versus time just inside the edge of the flux-conserver midplane; the electron temperature versus major radius; and the peak electron temperature versus time for a double-pulse experiment. The differences between the experimental data and the simulations are no worse than 25% and typically are much smaller. There are no major qualitative differences in the results compared. Although the diagnostics presently available on SSPX are not able to measure the detailed, local interior structure in the current and other parameters, these results strongly suggest

[a]Electronic mail: hooper1@llnl.gov
[b]Present address: University of Wisconsin, Madison, WI 53706.
[c]Present address: Department of Aeronautics and Astronautics, University of Washington, Seattle, WA 98195.

that the resistive MHD physics in the code is a good approximation to that in the experiment.

It should be kept in mind that the NIMROD description of the spheromak is an idealized model, and many pieces of physics are outside of its scope. For example, NIMROD does not include any model for the plasma sheath, nor does it include plasma sources and sinks (in the absence of which, the NIMROD continuity equation has an artificial diffusivity to keep the density reasonably smooth and to prevent any vacuum regions forming that would have divergent Alfvén velocities[11]). However, the work in Refs. 10 and 11 documents how well the relatively simple model of resistive, single-fluid magnetohydrodynamics in NIMROD captures the dominant behavior so far measured in the SSPX experiments and establishes the credibility of NIMROD as a research tool for providing insight into SSPX. In this document we therefore examine the physics of the reconnection process which converts toroidal flux into poloidal flux as seen in the simulation, show that the code predicts both voltage spikes on the cathode and the simultaneous growth of the poloidal field in a manner very similar to the experiment, and develop a set of predictions from the code to guide future experiments designed to examine this physics. The internal structure of the simulated plasma, including the locations and characteristics of current layers accompanying the reconnection, is one such prediction related to the reconnection processes and provides guidance for future internal probing of the experiment. (This has not been attempted to date because of the high plasma power density.)

The importance of reconnection in spheromaks has been known for some time. Ono *et al.* observed low-n kinks in the relaxation phase of the S-1 spheromak[12,13] and measured the resulting conversion of toroidal to poloidal magnetic flux, demonstrating the role of a tearing mode in the process. Yamada and co-workers[14,15] studied reconnection in the boundary layer between colliding spheromaks; among other results they demonstrated that the helicities of the spheromaks were additive during the reconnection and that substantial ion heating resulted from the magnetic-field annihilation.[16] Brown *et al.*[17] examined the generation of super-Alfvénic ions by reconnection at the interface of two spheromaks in the Swarthmore Spheromak Experiment (SSX) and modeled the physics with a $2-1/2$D code. Ji *et al.*[18] used magnetic probes to examine the structure of the reconnection in the two-dimensional interface between two spheromak-like plasmas, concluding that it was explained by a generalized Sweet–Parker model.

In the work in Ref. 15, current sheets were observed in the reconnection layer between colliding spheromaks with negative toroidal current relative to the initial toroidal currents. The reversed current appeared to be closely coupled to the reconnection process. The authors of Ref. 15 also show that the reconnection rate increases with the speed at which the spheromaks approach one another and suggest that this implies a role of current-sheet compression. In SSX the structure of the azimuthal current layer between colliding spheromaks had a central peak reversed relative to the current outside this layer.[19]

Reversed parallel current densities were also measured in two spheromaks, the Spheromak Experiment (SPHEX) and the Flux Amplification Compact Toroid[20] (FACT) using the probes located between the wall and $R/2$ with R the flux-conserver radius. The plasmas were more strongly driven than SSPX and considerably less symmetric, with magnetic-field fluctuation levels $\sim 10\%$, and the current reversal occurred sporadically. The local reversal of the current direction likely occurred when the large amplitude motion of the return current column moved it across the probe position rather than in a current sheet associated with reconnection.

A current sheet has also been studied during spontaneous reconnection in the Madison Symmetric Torus (MST) reversed-field pinch.[21] It was located at the $q=0$ (reversal) surface and was found to have a toroidal mode number $n=-1$ and a broad structure with a width of order the ion skin depth, greater than expected from linear two-fluid theory. The results are complementary to those in the spheromak in that the ohmic drive in the reversed-field pinch (RFP) injects poloidal flux which is converted into toroidal flux by reconnection. In the RFP this occurs in "sawtooth" bursts; in this work we suggest that reconnection in the spheromak is also a relaxation process and results in the observed spikes in the cathode voltage.

II. VOLTAGE SPIKES AND POLOIDAL FLUX GENERATION

Figure 1(a) shows the SSPX flux-conserver geometry and bias magnetic-flux contours. The computational geometry is very close to the experimental although it is inverted. The first 0.3 ms of startup voltage, current, and poloidal magnetic field in the SSPX spheromak are shown in Fig. 1(b). A very similar startup history found in the NIMROD code is also shown and helps clarify the physics processes. To obtain these results, the experimental geometry was nearly identical to the experiment as noted above, and the bias poloidal magnetic flux was modeled accurately by a set of coils. (Throughout this paper toroidal and poloidal fluxes refer to azimuthal averages, determined from the $n=0$ toroidal Fourier component.) The gun current prescribed in the simulation is a numerical fit to the experiment and is accurate to within 3%. No other time histories are imposed in the simulation. The boundary conditions on the flux conserver are $\mathbf{E}\times\hat{\mathbf{n}}=\delta\mathbf{B}\cdot\hat{\mathbf{n}}=\delta\mathbf{v}=\nabla n\cdot\hat{\mathbf{n}}=\delta T=\mathbf{0}$, where $\hat{\mathbf{n}}$ is the normal to the surface, $\mathbf{E}$ the electric field, $\delta\mathbf{B}$ the change in magnetic field from the bias, $\delta\mathbf{v}$ the change in fluid velocity, n the density, and δT the change in temperature; their implementation is discussed in Ref. 8. The density is nearly constant (5×10^{19} m^{-3}) for the reasons discussed in the Introduction and in Ref. 11. As discussed in the Appendix, a plasma rotation has been imposed at the boundary to approximately match the experimental observations. This is found to have little effect on plasma quantities. Also, the results are found to be insensitive to the magnitude of viscosity, as also discussed in the Appendix.

Along the insulating break between the cathode and the flux conserver, the symmetric component of B_ϕ is determined by the injector-current wave form with all of the gun current localized at R_{gun} at the bottom as the simulation ge-

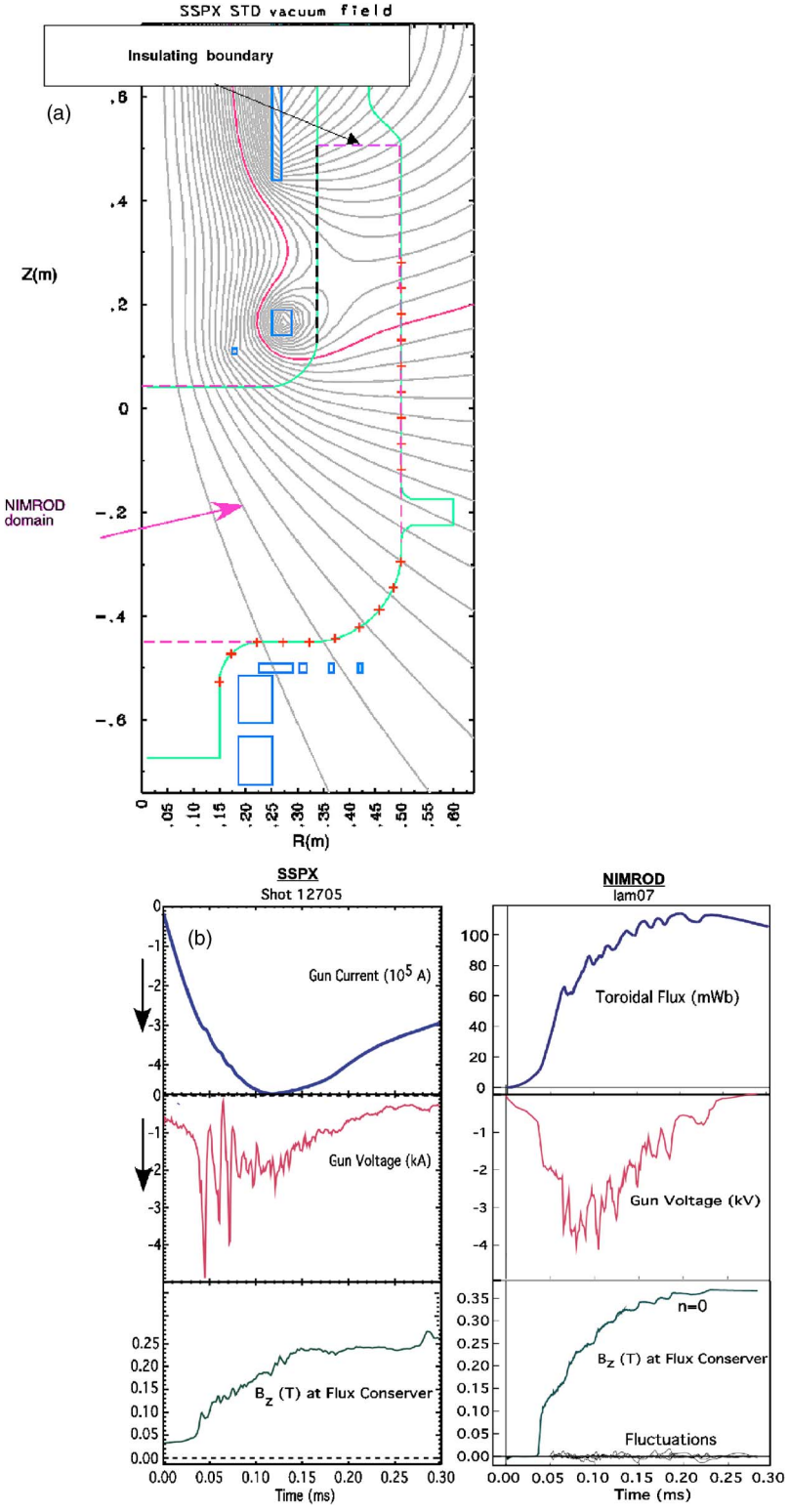

FIG. 1. (Color online). (a) SSPX flux-conserver geometry showing bias magnetic flux. The radius of the inner electrode (cathode) at the insulating boundary is R_{gun} and the outer electrode is R_{FC}. The NIMROD domain includes an insulating boundary which approximates the experimental insulator which is at the top of the flux conserver. (b) Time history of the plasma startup in SSPX (left) and in NIMROD (right). The current history in NIMROD is programmed to duplicate that in the experiment. To make this comparison, the initial mode amplitudes in the code were as large as convergence would permit, about 1% of the energy of the $n=0$ component. The initial rise in voltage, azimuthally averaged toroidal flux, and magnetic field are due to the "bubble burst" from the gun; the subsequent drops in toroidal flux are accompanied by step increases in poloidal magnetic field and azimuthally averaged poloidal flux (not shown). (Adapted from Ref. 11.)

ometry is inverted from the experiment shown in Fig. 1. Thus, along the insulating gap, $B_\varphi=\mu_0 I_{\mathrm{gun}}/2\pi R$ for $R_{\mathrm{gun}} \leqslant R \leqslant R_{\mathrm{FC}}$, as shown in the figure. The temperature in the bottom row of elements is kept at the ambient value to keep the resistivity high near the wall including the insulating boundary, allowing the current density to lift off the break. Maxwell's equations determine the electromagnetic fields along the insulating boundary subject to the condition that no current crosses the boundary except at the corner with the inner electrode. The cathode voltage is determined self-consistently from the response of the simulated plasma in the flux conserver to the applied current and internal processes and is calculated directly from the electric field integrated along a path across the gun, from one electrode to the other $V=\int \mathbf{E}\cdot\mathbf{d}\ell$.

In our simulations of SSPX we have made numerous numerical convergence studies. These include varying the mesh of finite elements from 16×36 to 24×48, the basis

functions for the elements from bilinear (second-order accurate) to bicubic (fourth-order accurate) to biquartic (fifth-order accurate), the maximum toroidal harmonic from $n=5$ to $n=21$, and the viscosity from 100 to 1000 m^2/s. Our convergence studies are incomplete, and not all the above studies have been applied to all physics regimes, but we have not found any significant qualitative differences in results going to higher resolution. There are observable quantitative differences, but they are not large.

The applied (bias) poloidal flux is ejected from the gun in a "bubble burst"[1] which results in the initial increase in toroidal flux and in the poloidal field at the wall; this will be illustrated by the results from the simulation in Sec. III. This ejection is seen clearly in the simulation as the initial step in gun voltage and magnetic field at $t \approx 0.035$ ms. The experimental ejection is not as clear from the voltage, probably because the early-time breakdown processes in the gun are highly nonaxisymmetric, but can be seen in the step at $t \approx 0.035$ ms in the poloidal magnetic field measured at the flux conserver. (The efficiency of poloidal field flux amplification in the experiment is somewhat less than in the simulation, likely for similar reasons.)

Examination of the numerical results shows that the poloidal flux during this process is nearly constant at the bias value even though the field is being redistributed in space. Once the plasma pinches and axisymmetry-breaking modes grow to appreciable amplitudes, a series of bursts occurs during which the toroidal flux decreases as seen in Fig. 1, starting at $t \approx 0.062$ ms in the simulation, and the poloidal field and flux increase and voltage spikes appear on the cathode. We suggest that the change in topology results from the reconnection events that we examine in detail in the simulation.

During these events, the energy in the axisymmetry-breaking modes decreases significantly, as can be seen in the isolated event discussed in Sec. III. The next event is delayed until the modes reach an amplitude similar to that of the previous one. The reconnection during spheromak formation is thus best described in terms of discrete relaxation events rather than a continuous, turbulent-like process, resulting in the voltage spikes seen on the cathode.

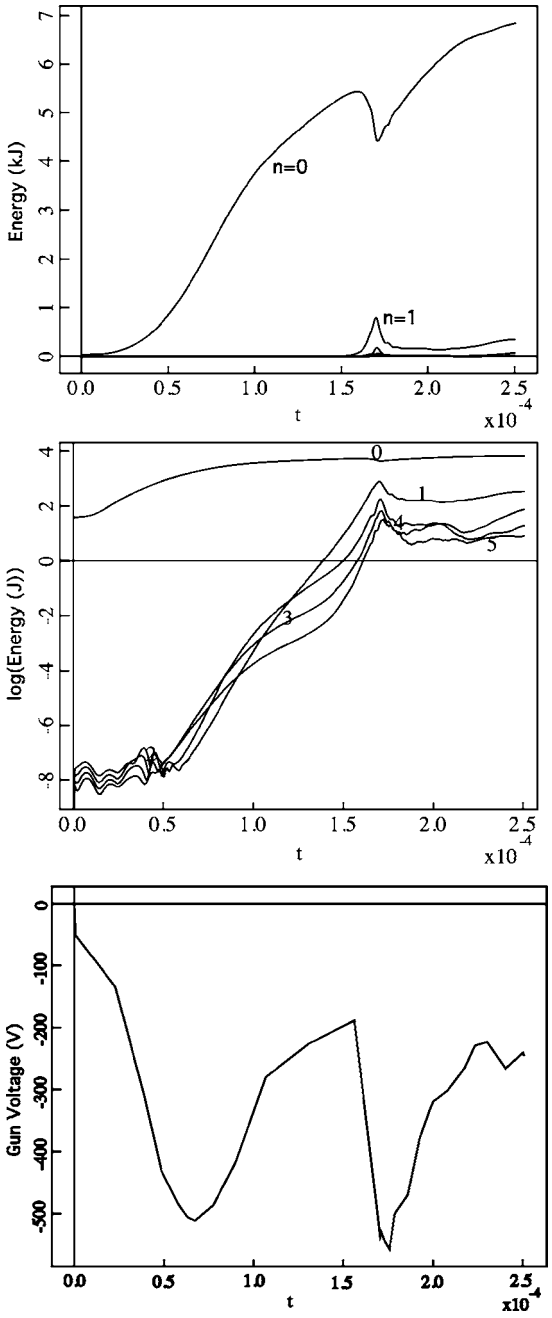

FIG. 2. Magnetic energy in the axisymmetric ($n=0$) and nonaxisymmetric ($n=1$–5) modes in the analyzed simulation run. The reconnection event starts at about 150 μs, and the energy in the axisymmetric component is converted into nonaxisymmetric modes and thermal energy. Linear scale (top). Logarithmic scale (middle) showing the mode growth. Also shown (bottom) is the gun voltage showing the voltage spike occurring during the reconnection event; compare to Fig. 1.

III. 3D RECONNECTION PHYSICS MODELED BY NIMROD

In application of NIMROD to SSPX, two-fluid effects are neglected but the large differences between heat conduction along and across magnetic fields are included. This anisotropy is important to modeling temperature profiles accurately, and during reconnection the relatively cold and resistive plasma on short, open field lines is important to accurate magnetic-field modeling.[10,11] Additional physics parameters used in the present calculation are listed in the Appendix.

To examine the reconnection physics, we analyze a different simulation run shown in Fig. 1, in which a single reconnection event occurs thereby allowing an easier isolation of the processes of interest. The event discussed here occurs when the code is initialized with a low amplitude for the MHD modes, unlike the experiment where the lack of symmetry during breakdown generates high initial amplitudes. (The initial "seed" energy in the modes is 10^{-3} of that in the simulation in Fig. 1.) As a result the first reconnection event occurs after the peak of the formation current, as can be seen by comparing Fig. 2 to the gun current in Fig. 1. In the experiment and high-seed energy simulation, reconnection starts before the gun current peaks.

The plasma bubble "blown" from the gun by the discharge current is seen in Fig. 3, timed just before the recon-

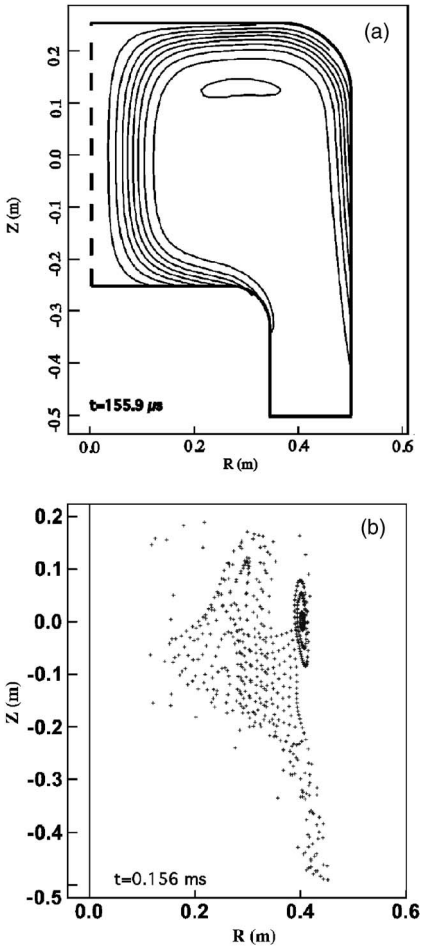

FIG. 3. Simulation results: (top) toroidally averaged poloidal flux and (bottom) field line Poincaré plots early in the reconnection event (156 μs). The puncture point structure arises because the magnetic field is primarily toroidal in the volume "inside" the poloidal flux contours, so field lines puncture the $\varphi=0$ plane many times before leaving the flux conserver. In the code the flux conserver is inverted from the experiment.

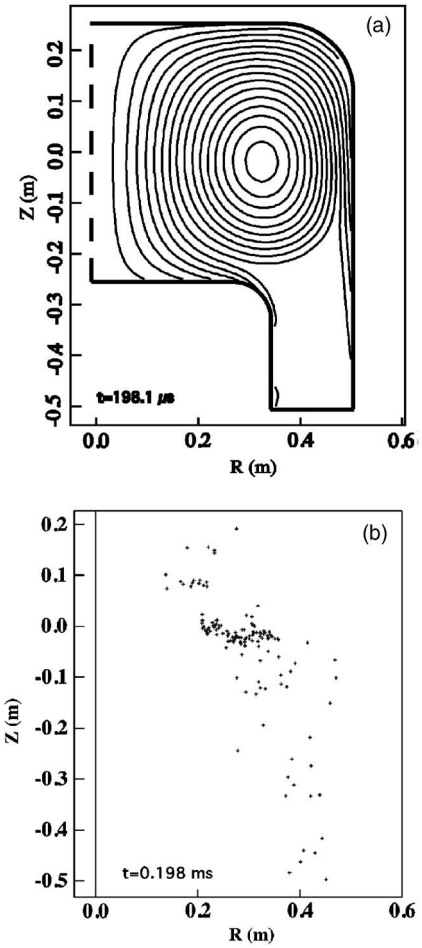

FIG. 4. (a) Toroidally averaged poloidal flux and (b) field line Poincaré plots late in the reconnection event (198 μs).

nection commences. The resulting configuration is nearly axisymmetric, and the Poincaré plot confirms that the magnetic field lines are open (connecting the electrodes). The puncture plot at $\phi=0$ has a regular pattern showing that at this time the field lines are not chaotic.

Because of the large current, the magnetic field pinches along the geometric axis, and after about 50 μs symmetry-breaking magnetic modes begin to grow. Figure 2 includes the energy in the azimuthal modes used in this calculation, $n=0$–5. At about 150 μs the symmetry-breaking modes reach sufficiently large amplitude that a strong reconnection event occurs. Similarities with the experiment, Fig. 1, include a voltage spike on the gun; cf. Fig. 2(c). There is a rapid conversion of azimuthally averaged toroidal flux into azimuthally averaged poloidal flux. Associated with this conversion are localized current sheets and a transition to a chaotic magnetic field.

At the beginning of the event the poloidal flux approximately equals the applied bias; by the end a good, mean-field (toroidally averaged) spheromak has formed. Figure 4 shows the contours of constant toroidally averaged poloidal flux and the associated field line Poincaré plots as the event nears completion. There has clearly been a transition to chaotic behavior. The resulting state has been characterized as "non-hyperbolic chaotic scattering" by Finn *et al.*[22] The chaotic transition can also be seen by tracing a set of field lines from the outer flux conserver to the cathode. In Fig. 5 the ending poloidal positions of the lines are seen to begin to move erratically as the reconnection event starts, where the poloidal position is defined as $lpf(i)=\sqrt{rc(i)^2+zc(i)^2}$ with $rc(i)$ and $zc(i)$ the intersections of line i with the cathode. Note that the field lines that start in the gun (e.g., $i=15$) begin to move before those outside the gun. These lines form the inside of the bubble seen in Fig. 3.

Examples of detailed field line behavior are shown in Fig. 6. During the initial flux balloon formation, lines in a "bundle" evolve close together. During reconnection, they become sensitive to details of the magnetic field along the trajectory; even small, localized changes in field can cause significant changes in the trajectory. Furthermore, because the field becomes chaotic, reconnection at small spatial scales leads to dramatic changes in field line trajectories on very short time scales; in the code, qualitative changes are observed in single time steps of 4 ns. Some field lines are found to form loose knots [Fig. 6(d)], a topological change that requires reconnection. It is clear, in fact, that at least

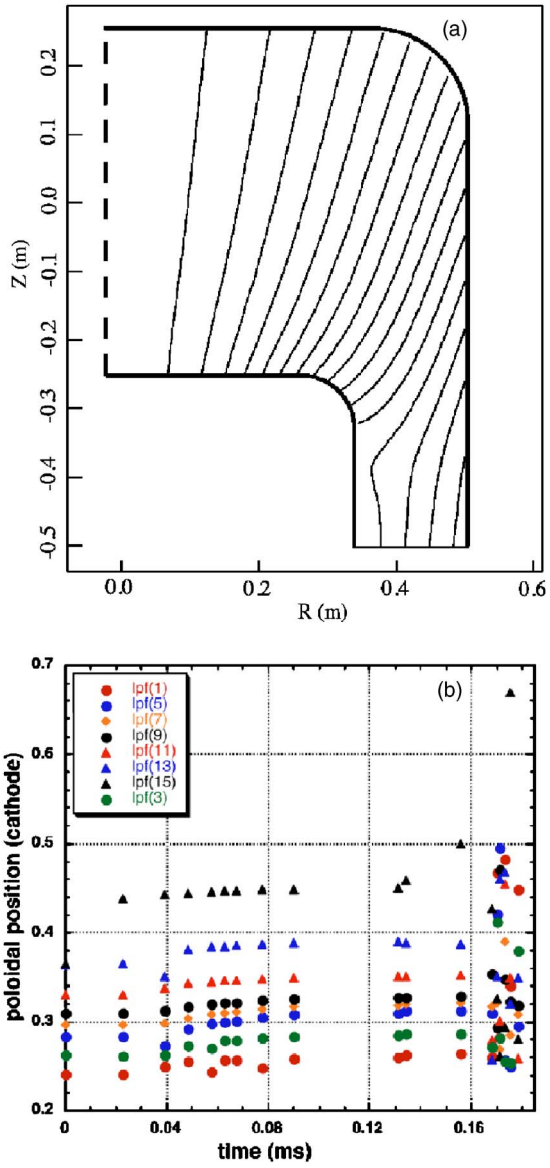

FIG. 5. (Color online). (a) Vacuum field lines. (b) Poloidal position on the cathode. Half the lines are shown, with $i=1$ the line which starts closest to the geometric axis on the flux conserver.

some of the field lines undergo multiple reconnections along their trajectory.

During the reconnection event, field lines starting 1 cm apart on the flux-conserver surface can separate and go to end points separated by significant distances, indicative of the chaotic nature of the process. An example is shown in Fig. 7 for the same field lines that form the bundle in Fig 6. The lengths of field lines which are initially close together differ by amounts which can become large (compared with the flux-conserver dimensions) characteristic of the transition to chaos. The mean-field structure has not changed significantly in this time; rather the lines have become sensitive to small, localized structure in the field. Much of the length difference results from differences in the number of toroidal transits the lines take before reaching the cathode.

The source of both the reconnection and the chaotic behavior of the field lines lies in the breaking of the axisymmetry by the magnetic fluctuations, with the $n=1$ mode dominating (Fig. 2). It is clear from the field line behavior, however, that there is fine structure associated with the reconnection. We have, therefore, examined details in the fields and currents from NIMROD. Figure 8 shows the spatial behavior of λ at a specific time and varying toroidal angle during the event. The region of strong reconnection shows an $n=1$ structure, consistent with the dominant MHD mode.

The regions of yellow contours correspond to negative values. The magnetic field does not reverse sign, so these correspond to negative current density. The negative current sheet is most intense at $\phi=0$ at this time in the discharge. As all the field lines are open (and thus connect the flux conserver and cathode), this requires cross-field currents, which can be seen in the NIMROD output. Furthermore, the strongest current sheets are localized inside the separatrix near the X point of the mean-field spheromak. They become broader away from an azimuth of maximum current intensity; c.f. Fig. 8, for example. Perpendicular fluid flows, Fig. 9, become large around the current sheet. The region of large perpendicular flow near the geometric axis has an $n=1$ structure but there is no current sheet associated with it. It therefore appears to be associated with the large-scale structure of the $n=1$ mode rather than reconnection processes. The current-sheet widths are within a factor of 2–3 of the spatial resolution, as discussed in the Appendix; we have not explored their detailed structure in these simulations.

Near the negative current locations, field lines which are initially close together begin to separate significantly, indicating that the reverse currents (and the inductive electric fields required to drive them) are associated with the reconnection processes. Gradients of current density in the regions of maximum intensity are typically $\Delta\lambda/\Delta x \sim 2000\ \mathrm{m}^{-1}/\mathrm{m}$, two orders of magnitude larger than the ratio of the flux-conserver eigenvalue to the flux-conserver radius. Magnetic diffusion rates will scale approximately with this ratio. As reconnection is essentially diffusive (at small distances) in the single-fluid, resistive MHD approximation, this is indicative of processes two orders of magnitude faster than those that occur on the global scale. At these times during the modeling, $T_e=20$–30 eV and $\eta \sim 10^{-5}\ \Omega\ \mathrm{m}$. The global profile changes in an L/R time $\sim \mu_0/\eta\lambda^2 \sim 10^{-3}$ s. The local scale length yields an evolution about 20 times faster, $\sim 50\ \mu$s. This time is consistent with the duration of reconnection events in both experiment and NIMROD as seen in the voltage spikes during experimental startup when there are relatively large initial mode amplitudes because of breakdown processes.

The azimuthally averaged ($n=0$) value of λ, shown in Fig. 10(a), provides an indicator of the most intense region of reconnection. Figure 10(b) shows the azimuthally averaged poloidal flux. Comparison of these two confirms the observation that the current sheets are above but near the separatrix of the mean-field spheromak. The reconnection can be thought of as feeding the converted flux into the spheromak which continues to grow as long as the event continues. Flux conversion continues at a slower rate after the strong event discussed here, eventually being balanced

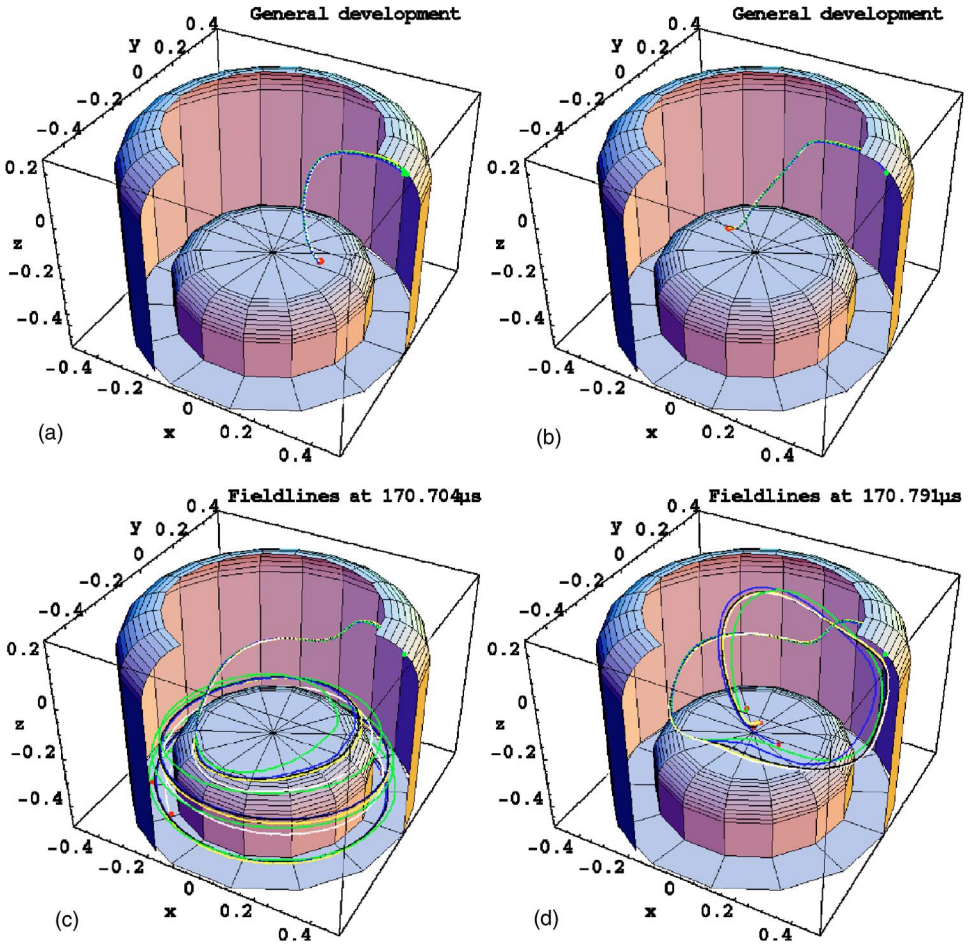

FIG. 6. (Color online). Traces of a bundle of five field lines within the spheromak flux conserver, initially spaced 1 cm apart in a cross on the flux-conserver surface. (a) The initial flux balloon from the gun pushes the field lines up against the flux conserver, $t=57.8064$ μs. (b) As current diffuses to radii inside the field line, the resulting toroidal field causes the lines to rotate around the geometric axis, $t=170.212$ μs. (c) As the reconnection proceeds, the field line geometries become quite complex, and the five lines behave differently, $t=170.704$ μs. (d) The field line topology change sometime generates knots, $t=170.791$ μs.

(and then dominated) by resistive decay later in the discharge as the mode amplitude decreases.[10,11]

Examination of vector plots of the fields generated by NIMROD reveals no magnetic field nulls near the mean-field *X* point, which have been posited by Lau and Finn as necessary for reconnection in the resistive MHD approximation.[23–25] Further, field lines were examined using Poincaré puncture plots. Extensive scans of starting points were made, including regions where the line returned one or a few times to within less than a centimeter of the initial point. In all cases, the puncture location subsequently deviates significantly from that location. Lengths of lines starting within 1 mm of each other often differ by meters (with the flux-conserver radius=0.5 m), consistent with the chaotic characteristics of the field. No evidence was found for closed lines at this point in the simulations. The breaking of the axisymmetry due to the $n=1$ mode and the current sheets is clearly strong enough to generate magnetic chaos. The field line behavior is similar to that of the linear, "short periodic spheroid" model of Lau and Finn,[24] in which regions of long field lines were found but there were no *X* lines or singularities. In effect, we have adopted the definition of reconnection due to Schindler *et al.*,[26] namely, a change in the connectiveness of highly separated plasma elements due to localized effects.

It is also of interest that the regions of negative λ show structure along the poloidal arc, with several peaks apparent in both the fixed and averaged azimuthal contour plots. Otto[27] made a similar observation in a model of reconnection in the resistive MHD approximation in the presence of a field component equivalent to the toroidal field in the spheromak. He found that if reconnection is triggered in a small region of an extended current sheet, it neither remains localized nor spreads into a long *X* line. He argues that the reconnection bends the field lines; the resulting magnetic tension cannot be balanced and the boundary between the reconnected line and its neighbors compresses, enhancing further reconnection in multiple patches which are essentially randomly distributed within the current sheet.

From the parallel component of Ohm's law, the reversal of λ in the NIMROD calculations implies a reversal of the local electric field relative to that elsewhere in the spheromak; this is presumably the induced field due to the change in magnetic topology associated with the reconnection event. Strong inductive electric fields in the reconnection layer are consistent with the generation of the high-energy ions observed in SSX (Ref. 17) and the ion heating typically observed during the formation of spheromaks. As the rate of change of helicity in the context of resistive MHD is

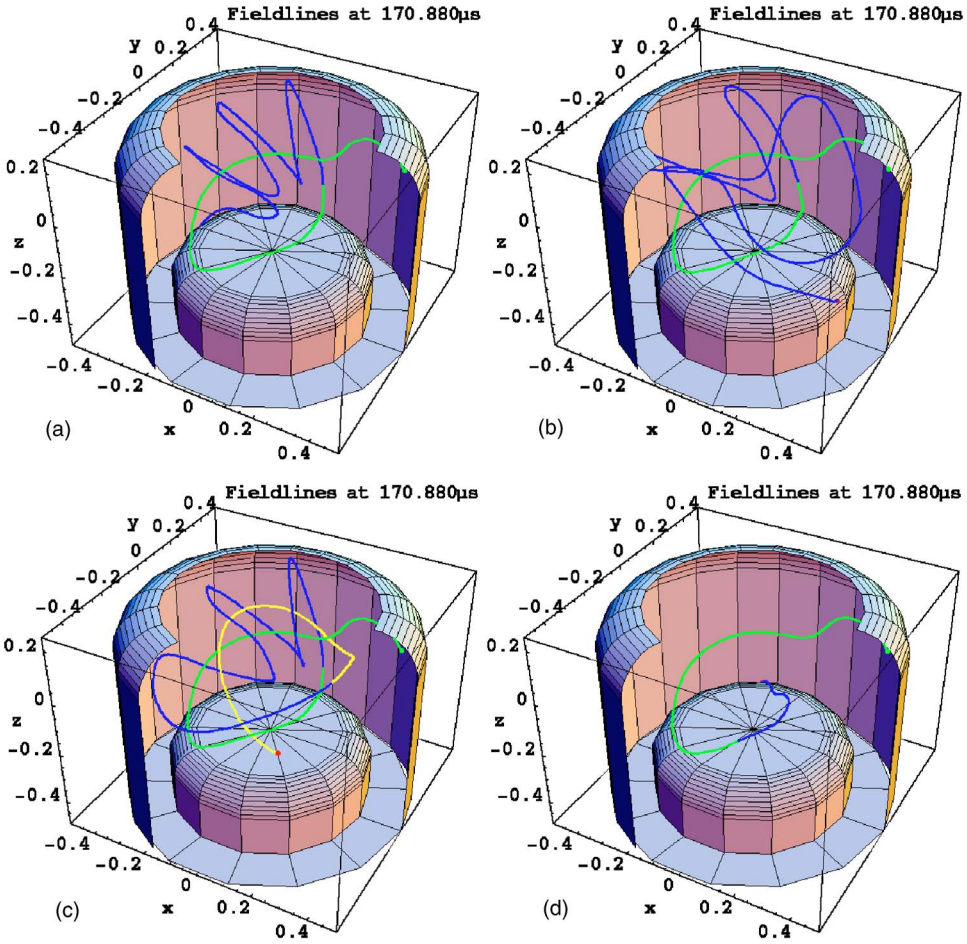

FIG. 7. (Color online). Four of the five fieldlines shown in Fig. 6 at 170.880 μs. The lines go to very different locations on the cathode. Four form complex knots; the fifth does not. Color changes along the field lines are used to clarify how the lines loop around themselves.

$$\frac{dK}{dt} = 2V_{\mathrm{gun}}\Psi_{\mathrm{gun}} - 2\int \eta\lambda B^2/\mu_0 dV,$$

the reversal of λ in the reconnection zone also implies a rearrangement of the helicity density within the volume. From the perspective of the external power system, the spheromak is behaving like an electric circuit dominated by inductance which is increasing with time[28] as reflected in the cathode voltage spikes. Schindler *et al.*[26] and Hess and Schindler[29] also emphasize the role of the parallel (to **B**) electric field in driving reconnection, although their model does not include the electrostatic driving term of the helicity-injected spheromak. In their case they envision a local dissipation of helicity due to the reconnection.

IV. CONCLUSIONS

A reconnection event in SSPX has been modeled using a resistive MHD code with the goal of generating insight into the local physics. The general agreement between the experimental observations during the event and the NIMROD model is good, although interior measurements have not been made in SSPX to date. Future experiments are planned for detailed comparison with the code. Predictions include negative current sheets close to the *X* point of the mean-field spheromak and the generation of chaotic field lines during reconnection events.

The modeling, which does not include two-fluid and kinetic effects, finds field line reconnection on the time scale of a few nanoseconds with the event lasting 10–100 μs. The reconnection is localized and fast relative to the large-scale evolution of the plasma, suggesting that details of the local physics may have little impact on the mean-field spheromak, and indeed the duration of the simulated reconnection event is about the same as in the experiment; and the generated poloidal flux is similar.

The details of reconnection during spheromak formation in the simulation are quite complex even though it neglects two-fluid and kinetic processes. The final spheromak is highly constrained by the flux conserver, however, and the mean-field geometry is surprisingly independent of the details even at the level of the internal gradient in λ. This results in part because fluctuations contribute quadratically to the azimuthally averaged equilibrium so that even a 10% fluctuation contributes to the force balance at only the 1% level.[30] This robustness also results because reconnection events—independent of their detailed physics—convert the injected toroidal flux into poloidal flux and build nearly identical large-scale configurations. The process, which conserves helicity better than magnetic energy, produces a final mean-field magnetic configuration not too different from Taylor's minimum-energy state[31] even when the actual field line structure is chaotic. The detailed physics is, of course, important for determining the final spheromak parameters.

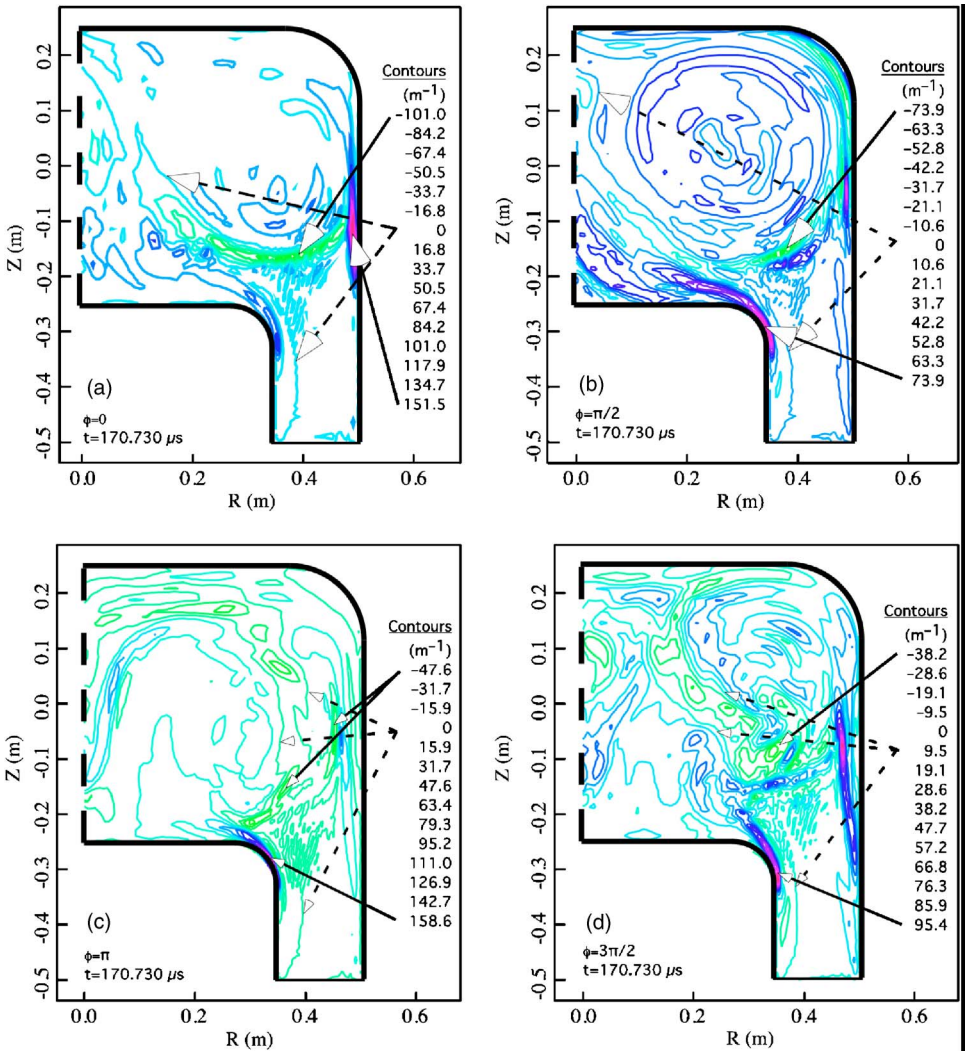

FIG. 8. (Color online). Spatial structure of λ. As the toroidal angle is changed in steps of $\pi/2$, the pattern shifts in response to the magnetic oscillation, dominated by $n=1$. The eigenvalue of the flux conserver is $\lambda_{fc}=9.6\ m^{-1}$, so the local departure from the Taylor state is very large.

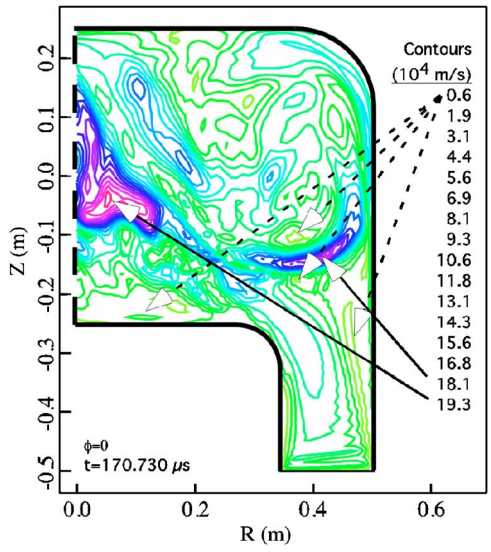

FIG. 9. (Color online). Velocity component perpendicular to the magnetic field at $t=170.730\ \mu s$ and $\phi=0$. Plasma rotation is applied to bring the mode frequencies into approximate agreement with experiment; this corresponds to $v_\phi=6.3\times10^4$ m/s at $R=0.5$ m.

For example, the dynamo term is of the same order as ηj in the parallel Ohm's law. The dynamo term therefore has a strong influence on the parallel current profile and on the final values of the toroidal current and other extensive spheromak variables.

ACKNOWLEDGMENTS

We greatly appreciate and have benefited from discussions with R. H. Cohen, J. M. Finn, T. K. Fowler, L. L. LoDestro, L. D. Pearlstein, and D. D. Ryutov.

The numerical simulations were performed at the National Energy Research Scientific Computing Center which is supported by the U. S. Department of Energy under Contract No. DE-AC03-76SF00098. This work was performed under the auspices of the U. S. Department of Energy by the University of California Lawrence Livermore National Laboratory under Contract No. W-7405-Eng-48 and by the U.S. Department of Energy through Grant No. DE-FG02-02ER54687 at the University of Wisconsin-Madison.

APPENDIX

Details of the NIMROD resistive MHD code can be found in Ref. 8 and the references therein. For the present

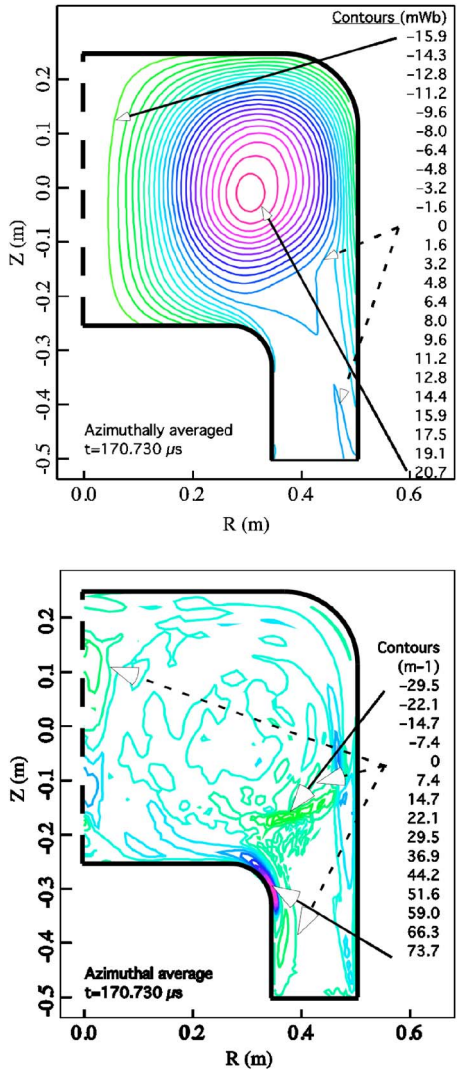

FIG. 10. (Color online) Contours of (a) azimuthally averaged poloidal flux and (b) azimuthally averaged λ.

calculations, the boundary matches that used in SSPX except that the coaxial region ("gun") between the cathode and anode/flux conserver was shorter in the second simulation. The bias magnetic field is generated by a set of coaxial coils as in SSPX, resulting in the "modified flux" configuration,[6] and the current pulse from the gun is a close approximation to that used in experiments. The poloidal plane is represented by a 16×32 mesh (normal×tangent to the electrode surfaces) of bicubic finite elements, and the toroidal direction is represented by finite Fourier series with $0 \leqslant n \leqslant 5$. The smallest length scale represented by bicubic elements is approximately the cell dimension divided by 3; in the present calculation the resulting resolution is $\leqslant 1$ cm throughout the computational regime. (In our simulation, the resistive layer width is $\sqrt{R\eta/v_A\mu_0} \sim 1$ cm in the low temperature, ~20 eV, open field-line regions.)

The calculation uses the single-fluid, single-temperature model with a large (artificial) density diffusion coefficient, effectively fixing the density throughout most of the flux conserver to within ~10% of 5×10^{19} m^{-3}. Density is swept out of the gun during formation, however, and deep in the gun is reduced by about 40% at the time of the reconnection event. Parallel thermal conductivity is modeled by a Braginskii electron approximation. Viscosity is modeled by a kinematic term, with a coefficient of 100 m^2/s. Simulations have ranged from 100 to 1000 m^2/s, with no qualitative changes, though the mode activity tends to be stronger, and the spheromak magnetic field larger at low viscosity. The calculations presented by Cohen *et al.* used 1000 m^2/s and the magnetic field at the flux conserver reached about 0.27 T. As shown in Fig. 1 of the present paper, our simulation obtained about 0.35 T. See also Ref. 32 for further discussion of the effect of viscosity on spheromak simulations.

An artificial rotation of 6.28×10^4 m/s at the flux-conserver outer wall (0.5 m) has been imposed, corresponding to an $n=1$ mode frequency of 20 kHz, approximately that observed in the experiment. The effect of this rotation propagation into the plasma is determined self-consistently by the simulation. In calculations without this, the rotation in the code is an order of magnitude less, and the physics generating this rotation in SSPX is believed to lie outside resistive MHD.[33] In tests using NIMROD, it was found that the rotation had little effect on the spheromak evolution, likely because the rotation speed is small compared with the Alfvén speed. The fluid rotated almost as a rigid body; otherwise, the fluid velocity contours nearly overlaid those without the additional rotation, and mode energies, q and λ values differed by ~10% or less.

[1] T. R. Jarboe, Plasma Phys. Controlled Fusion **36**, 945 (1994); see also references therein.
[2] J. B. Taylor and M. F. Turner, Nucl. Fusion **29**, 219 (1989).
[3] L. Lindberg and C. T. Jacobsen, Phys. Fluids **7**, S44 (1964).
[4] S. C. Hsu and P. M. Bellan, Phys. Rev. Lett. **90**, 215002 (2003).
[5] E. B. Hooper, L. D. Pearlstein, and R. H. Bulmer, Nucl. Fusion **39**, 863 (1999).
[6] H. S. McLean, S. Woodruff, E. B. Hooper, R. H. Bulmer, D. N. Hill, C. Holcomb, J. Moller, B. W. Stallard, R. D. Wood, and Z. Wang, Phys. Rev. Lett. **88**, 125004 (2002).
[7] C. W. Barnes, T. R. Jarboe, G. J. Marklin, S. O. Knox, and I. Henins, Phys. Fluids B **2**, 1871 (1990).
[8] C. R. Sovinec, A. H. Glasser, T. A. Gianakon, D. C. Barnes, R. A. Nebel, S. E. Kruger, D. D. Schnack, S. J. Plimpton, A. Tarditi, and M. S. Chu, J. Comput. Phys. **195**, 355 (2004).
[9] C. R. Sovinec, T. A. Gianakon, E. D. Held, S. E. Kruger, D. D. Schnack, and the NIMROD Team, Phys. Plasmas **10**, 1727 (2003).
[10] C. R. Sovinec, B. I. Cohen, G. A. Cone, E. B. Hooper, and H. S. McLean, Phys. Rev. Lett. **94**, 035003 (2005).
[11] B. C. Cohen, E. B. Hooper, R. H. Cohen, D. N. Hill, H. S. McLean, R. D. Wood, S. Woodruff, C. R. Sovinec, and G. A. Cone, Phys. Plasmas **12**, 056106 (2005).
[12] Y. Ono, R. A. Ellis, A. C. Janos, F. M. Levinton, R. M. Mayo, R. W. Motley, Y. Ueda, and M. Yamada, Phys. Rev. Lett. **61**, 2847 (1988).
[13] Y. Ono, M. Yamada, A. C. Janos, and F. M. Levinton, Phys. Fluids B **3**, 1452 (1991).
[14] M. Yamada, F. W. Perkins, A. K. MacAulay, Y. Ono, and M. Katsurai, Phys. Fluids B **3**, 2379 (1991).
[15] Y. Ono, A. Morita, M. Katsurai, and M. Yamada, Phys. Fluids B **5**, 3691 (1993).
[16] Y. Ono, M. Yamada, T. Akao, T. Tajima, and R. Matsumoto, Phys. Rev. Lett. **76**, 3328 (1996).
[17] M. R. Brown, C. D. Cothran, M. Landreman, D. Schlossberg, W. H. Matthaeus, G. Qin, V. S. Lukin, and T. Gray, Phys. Plasmas **9**, 2077 (2002).
[18] H. Ji., M. Yamada, S. Hsu, and R. Kulsrud, Phys. Rev. Lett. **80**, 3256 (1998).
[19] V. S. Lukin, G. Qin, W. H. Matthaeus, and M. R. Brown, Phys. Plasmas **8**, 1600 (2001).
[20] S. Woodruff and M. Nagata, Plasma Phys. Controlled Fusion **44**, 2539

(2002).
[21] N. A. Crocker, G. Fiksel, S. C. Prager, and J. F. Sarff, Phys. Rev. Lett. **90**, 035003 (2003).
[22] J. M. Finn, C. R. Sovinec, and D. del-Castillo-Negrete, Phys. Rev. Lett. **85**, 4538 (2000).
[23] Y.-T. Lau and J. M. Finn, Astrophys. J. **350**, 672 (1990); **366**, 577 (1991); Phys. Plasmas **3**, 3983 (1996).
[24] Y.-T. Lau and J. M. Finn, Astrophys. J. **366**, 577 (1991).
[25] Y.-T. Lau and J. M. Finn, Phys. Plasmas **3**, 3983 (1996).
[26] K. Schindler, M. Hess, and J. Birn, J. Geophys. Res. **93**, 5547 (1988).
[27] A. Otto, Astrophys. Space Sci. **264**, 17 (1999).
[28] S. Woodruff, B. I. Cohen, E. B. Hooper, H. S. McLean, B. W. Stallard, D. N. Hill, C. T. Holcomb, C. Romero-Talamas, R. D. Wood, G. Cone, and C. R. Sovinec, Phys. Plasmas **12**, 052502 (2005).
[29] M. Hesse and K. Schindler, J. Geophys. Res. **93**, 5547 (1988).
[30] D. D. Ryutov (private communication, 2004).
[31] J. B. Taylor, Phys. Rev. Lett. **33**, 1139 (1974); Rev. Mod. Phys. **58**, 741 (1986).
[32] C. R. Sovinec, J. M. Finn, and D. del-Castillo-Negrete, Phys. Plasmas **8**, 475 (2001).
[33] C. T. Holcomb (private communication, 2004).